

1 Sustained intensification of the Aleutian Low induces weak
2 tropical Pacific sea surface warming

3

4 William J. Dow¹, Christine M. McKenna¹, Manoj M. Joshi², Adam T. Blaker³, Richard Rigby¹,
5 Amanda C. Maycock¹

6

7 ¹School of Earth and Environment, University of Leeds, Leeds, UK

8 ²Climatic Research Unit, School of Environmental Sciences, University of East Anglia, Norwich,
9 UK

10 ³National Oceanography Centre, Southampton, UK

11

12 Correspondence: William J. Dow (earwd@leeds.ac.uk)

13

14

15 **Abstract**

16

17 It has been proposed that externally forced trends in the Aleutian Low can induce a basin-wide
18 Pacific SST response that projects onto the pattern of the Pacific Decadal Oscillation (PDO). To
19 investigate this hypothesis, we apply local atmospheric nudging in an intermediate complexity
20 climate model to isolate the effects of an intensified winter Aleutian Low sustained over several
21 decades. An intensification of the Aleutian Low produces a basin-wide SST response with a
22 similar pattern to the model's internally-generated PDO. The amplitude of the SST response in
23 the North Pacific is comparable to the PDO, but in the tropics and southern subtropics the
24 anomalies induced by the imposed Aleutian Low anomaly are a factor of 3 weaker than for the
25 internally-generated PDO. The tropical Pacific warming peaks in boreal spring, though anomalies
26 persist year-round. A heat budget analysis shows the northern subtropical Pacific SST response
27 is predominantly driven by anomalous surface turbulent heat fluxes in boreal winter, while in the
28 equatorial Pacific the response is mainly due to meridional heat advection in boreal spring. The
29 propagation of anomalies from the extratropics to the tropics can be explained by the seasonal
30 footprinting mechanism, involving the wind-evaporation-SST feedback. The results show that low
31 frequency variability and trends in the Aleutian Low could contribute to basin-wide anomalous
32 Pacific SST, but the magnitude of the effect in the tropical Pacific, even for the extreme Aleutian
33 Low forcing applied here, is small. Therefore, external forcing of the Aleutian Low is unlikely to

34 account for observed decadal SST trends in the tropical Pacific in the late 20th and early-21st
35 centuries.

36

37

38 Key points (140 chars)

39

40 1. A sustained intensification of the winter Aleutian Low produces weak warming in the
41 tropical Pacific that peaks in spring.

42 2. Changes to surface heat fluxes (subtropics) during boreal winter and meridional advection
43 (equatorial) during boreal spring in the upper ocean drive the SST warming.

44 3. A combination of the seasonal footprint mechanism and wind-evaporation-SST
45 mechanism generate the surface climate anomalies in the tropical Pacific.

46

47

48

49

50 1. Introduction

51

52 The Aleutian Low has a well-known role in determining the North Pacific component of the Pacific
53 Decadal Oscillation (PDO) (e.g. Schneider and Cornuelle, 2005; Zhang et al., 2018; Hu and Guan,
54 2018; Sun and Wang, 2006; Newman et al. 2016). Fluctuations in Aleutian Low intensity affect
55 the North Pacific subpolar gyre (Pickart et al. 2008), upper ocean temperatures (e.g. Latif and
56 Barnett, 1996) and sea surface height (Nagano and Wakita, 2019) through anomalous thermal
57 forcing and wind stress. Oceanic Rossby waves initiated by Aleutian Low variability can propagate
58 westward and cause lagged signals in the Kuroshio-Oshashio Extension (KOE) region (e.g.,
59 Kwon and Deser, 2007).

60

61 The traditional paradigm for the PDO describes the integrated effect of mid-latitude stochastic
62 variability, which induces SST anomalies through turbulent heat flux and wind stress curl
63 anomalies, and driving from tropical processes (ENSO variability) via excitation of Rossby wave
64 trains and tropical-extratropical teleconnections (Newman et al. 2016; Zhao et al. 2021; Vimont.
65 2005; Knutson and Manabe 1998; Jin 2001). We note that recent definitions separate low
66 frequency PDO variability and show this is predominantly associated with stochastic extratropical
67 atmospheric variability (i.e. the Aleutian Low) (Wills et al., 2018, 2019). However, decadal
68 changes in the Aleutian Low may arise via other mechanisms including Arctic sea ice trends
69 (Simon et al. 2021; Deser et al. 2016), stratospheric polar vortex variability (Richter et al., 2015),
70 or as a local response to external forcings (Smith et al. 2016; Dow et al. 2021; Dittus et al. 2021;
71 Klavans et al. submitted). It has been proposed that observed shifts in the PDO in the late 20th
72 and early 21st centuries were driven by anthropogenic forcing of the Aleutian Low, which was
73 then communicated to a basin-wide PDO signal (Smith et al. 2016; Klavans et al. submitted; Gan
74 et al. 2017). However, the mechanisms by which North Pacific anomalies linked to decadal
75 Aleutian Low changes may be communicated into a basin-wide SST response including the
76 tropics, and whether the amplitude of such a response matches observed variations, remain
77 unclear.

78

79 In this study, we aim to better understand the role of long-term changes in the Aleutian Low in
80 governing the multi-annual behaviour of tropical Pacific SSTs. We perform an ensemble of
81 atmospheric nudging simulations in an intermediate complexity coupled climate model to isolate
82 the effect of a sustained anomaly in the Aleutian Low. The response to this regional perturbation
83 is compared to the internally-generated low frequency Pacific variability in a free running

84 simulation. The manuscript is structured as follows: section 2 describes the methodology and
85 details of the model used. Section 3 compares the results of the nudging simulations with the free
86 running simulation. Discussion of the results is provided in section 4 and conclusions in section
87 5.

88

89 **2. Data and Methods**

90

91 **2.1 FORTE 2.0**

92

93 Simulations were performed using FORTE2.0, an intermediate complexity coupled Atmosphere-
94 Ocean General Circulation Model (AOGCM) (Blaker et al., 2021). The atmospheric model IGCM4
95 (Intermediate General Circulation Model 4) (Joshi et al., 2015) uses a truncated series of spherical
96 harmonics run at T42 resolution with 20 Σ -levels to a height of $\Sigma = 0.05$. IGCM4 is coupled to the
97 MOMA (Modular Ocean Model – Array) (Webb, 1996) ocean model run at $2^\circ \times 2^\circ$ resolution with
98 15 vertical levels. The two components are coupled once per day using OASIS version 2.3 (Terry
99 et al., 1999) and PVM version 3.4.6 (Parallel Virtual Machine). As described in Blaker et al. (2021),
100 between 5° N/S and the equator the horizontal ocean diffusion increases by a factor of 20 to
101 balance equatorial upwelling and parameterise the eddy heat convergence. For more details on
102 the model see Blaker et al. (2021). The model simulates multi-decadal SST variability in the
103 Pacific with a similar pattern to that seen in observations but a weaker amplitude by around a
104 factor of 4 to 5 (Figure S1). While the model is run at relatively low horizontal and vertical
105 resolution, the model code is sufficiently flexible to apply the nudging method described in Section
106 2.2 and the model is computationally efficient to run enabling a large ensemble to be produced.

107

108 **2.2 Grid-point nudging method**

109

110 Atmospheric nudging has been used to investigate climate and weather relationships between
111 remote phenomena (e.g. Martin et al., 2021; Knight et al., 2017; Watson et al., 2016). A nudging
112 code was added to IGCM4. Nudging was performed by adding tendencies to horizontal winds,
113 temperature and surface pressure. The nudging code is publicly available at
114 (<https://github.com/NOC-MSM/FORTE2.0>).

115 The nudging configuration is similar to that in Watson et al. (2016), with two additional terms to
 116 account for vertical (z) and temporal (t) variation in the nudging strength:

$$117 \quad \delta x(\lambda, \phi, z, t) = -\gamma(\lambda, \phi)g(z)h(t) \left(x(\lambda, \phi, z, t) - x_{ref}(\lambda, \phi, z, t) \right) / \tau, \quad (\text{Eqn 1})$$

118 where x is the variable being relaxed as a function of longitude (λ) and latitude (ϕ), x_{ref} is the
 119 reference state, and τ is the nudging strength (set to 6hr). The spatial extent of the nudging was
 120 tested extensively to avoid any shock at the boundaries and spurious effects of nudging near
 121 polar regions. The regional extent was determined as:

$$122 \quad \gamma(\phi, \lambda) = f_1(\phi, \phi_1, \phi_2)f_2(\lambda, \lambda_1, \lambda_2), \quad (\text{Eqn 2})$$

123 where

$$124 \quad f_1(\phi, \phi_1, \phi_2) = [1/(1 + e^{-(\phi-\phi_1)/\delta_1})][1 - 1/(1 + e^{-(\phi-\phi_2)/\delta_2})] \quad (\text{Eqn 3})$$

125 and

$$126 \quad f_2(\lambda, \lambda_1, \lambda_2) = [1/(1 + e^{-(\lambda-\lambda_1)/\delta_3})][1 - 1/(1 + e^{-(\lambda-\lambda_2)/\delta_3})] \quad (\text{Eqn 4})$$

127 $\Phi_1 = 30^\circ\text{N}$ and $\Phi_2 = 65^\circ\text{N}$ represent the southern and northern nodal points of the nudging region
 128 and $\lambda_1 = 160^\circ\text{E}$ and $\lambda_2 = 140^\circ\text{W}$ are the western and eastern nodal points of the nudging region.
 129 The coefficients $\delta_1 = 0.05$, $\delta_2 = 1$, $\delta_3 = 0.2$. The horizontal limits follow the commonly defined North
 130 Pacific Index (NPI) (Trenberth and Hurrell, 1994) as a proxy for the region encompassed by the
 131 Aleutian Low. Within the nudging patch shown in Fig. S2, the values are scaled so that the
 132 maximum value equals 1.

133 The temporal and nudging variations are determined as:

$$134 \quad g(z) = a \exp(-bz) \quad (\text{Eqn 5})$$

$$135 \quad h(t) = \exp\left(\frac{-d^2}{(2b^2)^{2\mu}}\right) \quad (\text{Eqn 6})$$

136 The strength of the tropospheric nudging is set to 1 (constant a , Equation 5) at $z = 0.96$ (lowest
 137 atmospheric level), decreasing exponentially to 0 at $z = 0.05$ (tropopause) (Equation 5). Nudging
 138 is applied during the extended boreal winter season (NDJFM) peaking on 15 January, with a
 139 Gaussian function in time to increase the nudging strength from 0 to 1 between 1 to 30 November

140 and a reverse ramp-down during March. Term d (Equation 6) is the time difference relative to
141 maximum nudging time in months (e.g. $d = 0$ on 15th Dec, $d = -1$ on 15th Jan, etc.), β is a constant
142 set to 1.2, μ is a constant set to 2. Outside of the nudging window, $h = 0$. The spatio-temporal
143 forms of the nudging coefficients are shown in Figure S2.

144
145 The strong Aleutian Low state is taken from a 100 year long control run (CONTROL) based on a
146 winter month with an NPI anomaly of -10.76 hPa, or -3.02σ , where $\sigma = 3.53$ hPa is the standard
147 deviation calculated over all winter months in CONTROL (Figure S3). Therefore, the target state
148 represents an extreme intense Aleutian Low state as simulated in FORTE2.0. Comparing with
149 ERA5 reanalysis data from 1979-2020, a 1σ NPI anomaly is 5.20 hPa. The imposed
150 atmospheric forcing is therefore weaker than if an equivalent experiment was conducted using a
151 comparably sized NPI anomaly in reanalysis data. A 50 member NUDGED ensemble was
152 generated using initial conditions drawn from each January 1st of the final 50 years of
153 CONTROL. Each member is integrated for 30 years with nudging commencing on 1 November
154 of the first year and repeating each winter of the simulation. Unless otherwise stated, the
155 analysis shows ensemble mean anomalies in the NUDGED simulation compared to the long-
156 term climatology of CONTROL. Statistical significance of the ensemble mean difference is
157 estimated as being where the anomaly ± 2 standard errors does not overlap zero. Standard error
158 (SE) is calculated as

$$159 \quad SE = \sigma/\sqrt{n} \quad (\text{Eqn. 7})$$

160 Where σ is the inter-ensemble standard deviation of the time averaged anomaly of interest and
161 n is the ensemble size, 50.

162 **2.3 Mixed Layer Heat Budget Analysis**

163 The heat budget of the upper 30m of the ocean (representing the mixed layer) is analysed for the
164 regions shown by the boxes in Figure 1, where the temperature tendency is given by:

$$165 \quad dT/dt = ADV + DIFF_{\text{vert}} + DIFF_{\text{horiz}} + CONV \quad (\text{Eqn. 8})$$

166 Daily tendencies due to advection (ADV), vertical and horizontal diffusion ($DIFF_{\text{vert}}$ and $DIFF_{\text{horiz}}$)
167 and convection (CONV) are output from the model. Further granularity in the heat budget terms
168 (e.g. turbulent fluxes) was not possible due to the limited availability of diagnostics from the

169 model. Vertical diffusion represents the contribution to the mixed layer heat budget from surface
170 turbulent and radiative fluxes. ADV is composed of zonal, meridional and vertical components:

$$171 \quad ADV = u \frac{\delta T}{\delta x} + v \frac{\delta T}{\delta y} + w \frac{\delta T}{\delta z} \quad (\text{Eqn. 9})$$

172 where u , v and w are the zonal, meridional and vertical components of the ocean velocity and
173 dT/dx represents the local zonal gradient of temperature. We linearize the meridional advection
174 term to investigate the relative roles of changes to ocean current velocity and temperature
175 gradient as follows:

$$176 \quad \left(v \frac{\delta T}{\delta y} \right)' = v' \frac{\delta T_0}{\delta y} + v_0 \left(\frac{\delta T}{\delta y} \right)' + v' \left(\frac{\delta T}{\delta y} \right)' \quad (\text{Eqn. 10})$$

177 where the subscript 0 denotes CONTROL values and primes denote anomalies in NUDGED.

178 **2.4 PDO Index**

179 The PDO index is calculated as the first EOF of monthly SST anomalies, calculated as deviations
180 from the climatological seasonal cycle, over the region 20-65°N, 120-260°E (Mantua et al. 1997).
181 Before calculating the leading EOF, the temperature anomalies are weighted by the square-root
182 of the cosine of latitude to account for the decrease in area towards the pole. The monthly principal
183 component, corresponding to the PDO index, is normalised by the standard deviation to give it
184 unit variance. The pattern of temperature anomalies that covaries with the PDO is found by
185 linearly regressing the time series of the monthly mean temperature anomalies onto the monthly
186 PDO index (Figure 1b). Here we define the PDO using the common index based on the leading
187 EOF of North Pacific SST variability. Wills et al. (2019) showed that the tropical Pacific SST
188 anomalies associated with this index are predominantly related to high frequency (e.g., ENSO)
189 SST variability, while the extratropical part is related to turbulent heat flux and wind stress
190 anomalies associated with intrinsic Aleutian Low variability. The discrepancy between the
191 modelled and observed SST anomalies associated with the PDO index in Figure S1 could be due
192 to the slightly weaker than observed ENSO amplitude in the model by around 33% (Figure S4)
193 (see also Blaker et al., 2021).

194 **3. Results**

195

196 *3.1 Surface temperature response*

197 Figure 1a shows annual mean surface temperature anomalies in NUDGED expressed as a
198 change per standard deviation (σ) of the PDO index. Here, the anomaly between NUDGED and
199 CONTROL is projected onto the first EOF from the control run to generate a pseudo-PC. The
200 anomaly is divided by the pseudo-PC to calculate the anomaly per standard deviation of the PDO
201 index, expressed in a similar way to that derived from CONTROL. A horse-shoe pattern of
202 anomalous temperature extends across the North Pacific, comprising warming in the north and
203 eastern Pacific and along the west coast of North America and cooling in the western North
204 Pacific/KOE region. The strongest warming (0.2-0.3 K/ σ) is seen over the North Pacific and
205 western North America. There is weaker (0.02-0.04 K/ σ) but statistically significant warming in the
206 equatorial Pacific. Across the Pacific Ocean, the pattern of temperature anomalies in NUDGED
207 closely resembles unforced multidecadal Pacific variability in CONTROL (Figure 1b), with a
208 pattern correlation coefficient of 0.53. Therefore, a sustained increase in Aleutian Low strength
209 forces a basin-wide SST response which resembles that associated with internally-generated
210 coupled variability in CONTROL. However, there are clear differences in the sign of the anomaly
211 outside the North Pacific basin and nudging region, such as over north-eastern Siberia and south-
212 central USA. Furthermore, while the extratropical SST anomalies are somewhat larger in
213 NUDGED, particularly in the subpolar gyre, the tropical Pacific signal is substantially weaker by a
214 factor of ~ 3 . This indicates that atmospheric forcing by the Aleutian Low alone is not sufficient to
215 generate a basin-wide SST response that is consistent with the intrinsic variability of the model.
216 Note the Aleutian Low state in x_{ref} is extreme (-3σ), meaning a more realistic amplitude for
217 sustained Aleutian Low intensification can be expected to induce a weaker response.

218 The seasonality of the surface temperature anomalies in NUDGED is shown in Figure 2 separated
219 for years 1-2, years 3-4 and years 5-30. The initial response to the intensified Aleutian Low is a
220 warming in the subpolar gyre in boreal autumn (SON). This amplifies in DJF during the peak of
221 the nudging period, where a tongue of warming extends into the subtropical North Pacific. This
222 pattern persists into MAM after nudging ceases but is also accompanied by warming in the
223 eastern tropical Pacific. By JJA, the tropical and subtropical temperature changes have weakened
224 leaving residual warming in the subpolar gyre that persists into the following winter. The
225 temperature anomalies over land quickly dissipate due to the low specific heat capacity. A similar
226 seasonal evolution occurs in years 3-4, but the tropical warm anomaly emerges earlier in DJF
227 and extends further westward at its peak in MAM. The anomalies in years 5-30 show a similar
228 spatiotemporal pattern to the first 4 years, suggesting the mechanisms by which the anomalies
229 manifest do not evolve strongly when the signals are maintained over multi-year timescales. Small

230 differences between years 1-4 and 5-30 are the extent of the robust signal in the tropical Pacific;
231 there is a small reduction in the amplitude of the tropical warming in JJA and no significant western
232 tropical Pacific warming in MAM for years 5-30. The signal of peak tropical warming in MAM in
233 NUDGED qualitatively agrees with observed low frequency Pacific variability (Figure S1), though
234 we note that FORTE2.0 shows a narrower band of tropical warming compared to observations.
235 Furthermore, the weak (up to ~10x weaker) footprint of modelled PDO variability in the equatorial
236 Pacific (Fig. S1) is consistent with a notion that Aleutian Low driven SST variability in the extra-
237 tropics has little influence on tropical variability (Wills et al., 2019; Zhao et 2021).

238

239 *3.2 Mixed layer heat budget*

240 The mixed layer heat budget in the subtropical North Pacific and Niño 3.4 regions shows different
241 annual cycles in the anomalous temperature tendencies (Figure 3 a,b). The largest anomalous
242 surface temperature tendency in the subtropical North Pacific occurs during the nudging period
243 (DJF), whereas the peak warming tendency in the Niño3.4 region occurs in February-April. In the
244 subtropics in winter, warming from vertical diffusion is offset by meridional advection. In contrast
245 in the Niño 3.4 region, anomalous meridional advection contributes to a warming tendency year-
246 round, with the maximum (~0.3 K/month) in MAM. This warming is partly offset by anomalous
247 vertical diffusion and convection. Meridional advection therefore contributes to cooling in the
248 subtropical North Pacific but causes warming in the Niño 3.4 region.

249

250 The anomalous meridional advection in the subtropical North Pacific is dominated by the change
251 in meridional velocity, whilst in the Niño3.4 region the change in meridional temperature gradient
252 is the largest contributor throughout most of the year (apart from Sept-Dec) (Figure 3 c,d). The
253 enhanced warming tendency from Feb-June in the Niño3.4 region is driven by changes in
254 meridional velocity. The difference in contributing terms implies different mechanisms governing
255 the changing mixed layer temperatures in the two regions.

256

257 The net surface heat flux anomalies in NUDGED are shown in Figure 4(a-d). There are positive
258 (downward) net surface heat flux anomalies across the North Pacific and within a SW-NE oriented
259 band in the subtropical North Pacific. The largest heat flux anomalies occur during DJF, with
260 values in excess of $4 \text{ W m}^{-2}/\sigma$. The net surface heat flux anomalies in NUDGED are dominated
261 by the latent heat flux (Fig. 4 e-h). The pattern of surface latent heat flux anomalies in JJA in the

262 extratropical North Pacific represents a damping of the SST anomalies; positive flux anomalies
263 extend eastward from the KOE region, which are enveloped by negative anomalies in the
264 northeast Pacific and subtropical North Pacific.. The positive heat fluxes exhibited in the KOE
265 region in all seasons outside of DJF are evidence that cold SST anomalies in this region reduce
266 heat loss to the atmosphere throughout the simulations. Regions such as those in the north-east
267 North Pacific appear to dampen the SST anomalies during MAM and JJA, which may indicate
268 limited dynamic feedback to the atmosphere. However, across the central North Pacific, the
269 persistence of surface latent flux anomalies year-round is expected given the surface temperature
270 persistence and alludes to ocean-atmosphere feedbacks.

271

272 *3.3 Atmospheric circulation response*

273 Figure 5 shows the seasonal mean zonal and meridional near-surface wind anomalies in
274 NUDGED. As expected, the largest anomalies occur in the period over which nudging is applied
275 (DJF), with a westerly zonal wind anomaly of up to $\sim 0.5 \text{ ms}^{-1}/\sigma$ in the subtropics and an easterly
276 anomaly of a similar magnitude in the subpolar extratropics. The meridional wind shows
277 alternating southerly-northerly anomalies across the North Pacific orientated with a north-easterly
278 tilt suggesting that a persistently strong AL invokes a modulation of the climatological Rossby
279 wave train providing a pathway for atmospheric communication between the North Pacific and
280 eastern tropical Pacific. Evidence for the modulation of the Rossby wave train is further evident
281 in the upper tropospheric winds (Figure S5). Recall that the nudging strength in the upper
282 troposphere is several times weaker than at the surface (Fig. S2), so the upper-level circulation
283 anomalies likely represent a response to the lower tropospheric forcing. The subtropical zonal
284 wind anomalies represent a southerly shift of the westerlies compared to the climatology in
285 CONTROL, with persistent anomalies extending into the spring after nudging ceases (April – not
286 shown). Interestingly, there is an emergence of a westerly wind anomaly near the coast of Central
287 America in DJF that extends southward and westward into the equatorial Pacific in MAM.
288 Although zonal wind anomalies are evident in JJA, they are not strongly statistically significant.

289 Figure 6 shows the latitude-time evolution of surface temperature, near-surface wind and surface
290 pressure anomalies in NUDGED averaged over the central and eastern tropical Pacific (which is
291 entirely outside the nudging region). There is year-round warming in subtropical and equatorial
292 regions, with the largest magnitude in the subtropics from November through April ($\sim 0.05 \text{ K}/\sigma$)
293 and in the equatorial region from March through July ($\sim 0.3 \text{ K}/\sigma$). The nudging invokes concurrent
294 warming in the subtropics, while there is a seasonal delay in the emergence of warming in the

295 equatorial Pacific. From July to November in the subtropics (around 15°N) there is substantially
296 less warming than during the rest of the year, with values close to zero. The westerly wind
297 anomalies coincide with the timing of the temperature anomalies, with south-westerly anomalies
298 of $\sim 0.05 \text{ m s}^{-1}/\sigma$ in the subtropics and $\sim 0.03 \text{ m s}^{-1}/\sigma$ in the equatorial region. In addition to the
299 cross-equatorial temperature gradient generated by the subtropical anomaly, the lower surface
300 pressure in the northern subtropics ($\sim 1.5 \text{ hPa}$), which is largest in February and March, creates a
301 pressure gradient across the equator, a key component of the WES mechanism. At this time there
302 is evidence of cooling in the southern subtropics (south of 15°S).

303

304 **4. Discussion**

305

306 The impact of an intensified Aleutian Low on the tropical Pacific in this study suggests an
307 excitation of the SFM mechanism (e.g. Vimont et al. 2003; Alexander et al. 2010; Chen and Yu,
308 2020; Sun and Okumura, 2019). In accordance with the SFM, the SST anomalies persist into the
309 summer season, with anomalous temperatures found in the North Pacific year-round. The signals
310 in winter and spring show a similar spatial signature to that found by Liguori and Di Lorenzo
311 (2019), who show an SST signature in the subtropics as a precursor to ENSO dynamics. Here
312 we find a similar effect on multi-year timescales in response to an anomalous Aleutian Low.

313

314 The midlatitude westerly winds show a southerly shift throughout the year which, in agreement
315 with Liu et al. (2021), acts to prevent heat loss from the surface in the northern subtropics due to
316 reduced evaporation. This in turn drives the SST anomaly towards the equator. Liu et al. (2021)
317 show the SFM as the mechanism that propagates SST anomalies southward, through a change
318 in latent heat fluxes. However, in DJF the westerly winds imposed by the nudging cause a
319 weakening of the subtropical trades; hence the southerly shift of westerlies starts to occur within
320 the season of nudging. We show anomalous latent heat flux is responsible for the change in
321 subtropical North Pacific SSTs. The limitation of the Liu et al. (2021) study is that the atmosphere
322 was coupled to a thermodynamic slab-ocean, whereas we integrate a fully coupled ocean model
323 allowing for a role of ocean dynamical feedbacks. Sun and Okumura (2019) conducted a related
324 investigation by imposing heat flux anomalies associated with the North Pacific Oscillation (NPO)
325 , but they imposed a fixed year round anomaly whereas the Aleutian Low shows strongest
326 variability in winter and therefore we only impose relaxation during boreal winter in our
327 experimental design. The simulations presented use an anomalous Aleutian Low state taken from
328 a single month (Figure S3). An area for future research is to impose a suite of varying Aleutian

329 Low states with different spatial and temporal profiles to test the sensitivity of the responses
330 described here to details of the imposed relaxation state.

331
332 In the tropical Pacific, the dominant mechanism responsible for the increase in SSTs is meridional
333 advection, with the change to meridional current velocity driving the accelerated warming in boreal
334 spring. This coincides with an anomalous northward cross-equatorial SST gradient and the
335 development of an anomalous cross-equatorial southward pressure gradient. Cross-equatorial
336 winds are generated, which, due to Coriolis force act to weaken the trades in the northern
337 equatorial region, decreasing the surface latent heat flux and leading to a local warming. The heat
338 budget analysis shows that surface heat fluxes are the primary warming agent during the nudging
339 period, whereas a change to surface advection drives the warming in the central near-equatorial
340 Pacific. A comprehensive review of this mechanism, commonly referred to as the wind-
341 evaporation-SST (WES) mechanism, is provided in Mahajan et al. (2008). Further, the
342 mechanism has been posited as a pathway through which North Pacific SSTs can influence
343 ENSO variability (Amaya et al. 2019). The equatorial thermocline depth shows a slight deepening
344 of the thermocline in all seasons apart from SON, which is supported by changes in the vertical
345 advection term (not shown). Figure 7 gives a pictorial representation of the combined mechanisms
346 involved in translating the Aleutian Low anomaly into the deep tropics.

347
348 While the results make conceptual sense and are in broad agreement with studies using more
349 comprehensive modelling tools (see earlier references), the amplitude of the response could be
350 verified in other more detailed coupled climate models. The coarseness of the coupled model,
351 specifically the vertical dimension of the oceanic component, is a limitation of the study.
352 Furthermore, the model's relatively low resolution and inability to resolve mesoscale processes in
353 the ocean and atmosphere may affect the results of the study. Future studies using observations
354 and higher resolution GCMs to test the results herein would be valuable. Furthermore, to ensure
355 model stability, the anomalous nudging state was drawn from the coupled atmosphere-ocean
356 control simulation. The Aleutian Low variability sampled from this simulation therefore includes
357 effects from tropical variability. The month used as the reference state for the nudging coincides
358 with an ENSO state (magnitude = 0.55) in the tropical Pacific. Further study could investigate
359 more idealised AL states and their effects on extra-tropical-tropical communication.

360
361 **5. Conclusions**

362

363 Externally-forced Aleutian Low trends have been implicated as a potential driver of recent
364 variations in the Pacific Decadal Oscillation (Smith et al., 2016; Klavans et al., submitted). Here,
365 we have investigated the potential influence of Aleutian Low trends on basin-wide low frequency
366 Pacific sea surface temperature variability using nudging simulations in an intermediate
367 complexity climate model. The target Aleutian Low state represents an extremely intense Aleutian
368 Low state (-3σ of winter monthly variability) applied during boreal winter. The intensified Aleutian
369 Low induces a basin-wide SST response that resembles the model's internally-generated PDO
370 with a comparable amplitude in the extratropics, but a substantially weaker amplitude in the
371 equatorial Pacific by a factor of 4 to 5. The pattern of SST variability exhibited across the basin is
372 evident on interannual timescales as well as throughout the duration of the 30 year simulation.

373

374 The findings presented here support that the PDO can, at least in part, be driven by remotely
375 forced changes in the North Pacific atmospheric circulation independent of the tropics. However,
376 in our experiment the amplitude appears to be too weak to fully explain a multi-annual shift in the
377 PDO across the tropics. This suggests that the hypothesis posed by Smith et al. (2016), that
378 anthropogenically forced changes in the Aleutian Low drove the observed shift in the phase of
379 the basin-wide PDO in the late 20th and early 21st centuries, should be revisited.

380

381 **Code availability**

382

383 The nudging code used in the analysis can be found:

384 (<https://github.com/NOC-MSM/FORTE2.0>).

385

386 **Data availability**

387

388 Underlying model data found in this paper is available from the corresponding author upon
389 request.

390

391 HadISST data available: <https://www.metoffice.gov.uk/hadobs/hadisst/data/download.html>

392

393 **Author contribution**

394

395 WJD and ACM designed the study. WJD developed the nudging code in FORTE2.0 with support
396 from CMM, MMJ and RR. ATB and RR helped with installation of FORTE2.0 at Leeds. WJD

397 performed the analysis and produced the figures. WJD and ACM wrote the manuscript with
398 comments from all authors. All simulations were performed on the ARC4 HPC at the University
399 of Leeds.

400

401 **Competing interests**

402

403 The authors declare that they have no conflict of interest.

404

405 **Acknowledgements**

406

407 WJD was supported by a Natural Environment Research Council (NERC) Ph.D. studentship
408 through the SPHERES Doctoral Training Partnership (NE/L002574/1) and by a Met Office CASE
409 studentship. ACM and CMM were supported by the European Union's Horizon 2020 Research
410 and Innovation Programme under Grant Agreement 820829 (CONSTRAIN project). ACM was
411 supported by the Leverhulme Trust. We are grateful to Paloma Trascasa-Castro for discussion of
412 ENSO processes. We are grateful for feedback on an earlier version of this manuscript from John
413 Marsham and Laura Wilcox.

414

415 **References**

416

417 Alexander, M. A., & Deser, C. (1995). A mechanism for the recurrence of wintertime
418 midlatitude SST anomalies. *Journal of Physical Oceanography*, 25(1), 122–137.
419 [https://doi.org/10.1175/1520-0485\(1995\)025<0122:AMFTRO>2.0.CO;2](https://doi.org/10.1175/1520-0485(1995)025<0122:AMFTRO>2.0.CO;2)

420 Alexander, M. A., Vimont, D. J., Chang, P., & Scott, J. D. (2010). The impact of
421 extratropical atmospheric variability on ENSO: Testing the seasonal footprinting
422 mechanism using coupled model experiments. *Journal of Climate*, 23(11), 2885–
423 2901. <https://doi.org/10.1175/2010JCLI3205.1>

424 Amaya, D. J., Kosaka, Y., Zhou, W., Zhang, Y., Xie, S. P., & Miller, A. J. (2019). The North
425 Pacific pacemaker effect on historical ENSO and its mechanisms. *Journal of Climate*,
426 32(22), 7643–7661. <https://doi.org/10.1175/JCLI-D-19-0040.1>

427 Barnett, T. P., Pierce, D. W., & Planck, M. (1999). Interdecadal interactions between the
428 tropics and midlatitudes in the Pacific basin. *Geophysical Research Letters*, *26*(5),
429 615–618.

430 Blaker, A., Joshi, M., Sinha, B., Stevens, D., Smith, R., & Hirschi, J. (2021). FORTE 2.0: a
431 fast, parallel and flexible coupled climate model. *Geoscientific Model Development*,
432 275–293. <https://doi.org/10.5194/gmd-14-275-2021>

433 Chen, S., & Yu, B. (2020). The seasonal footprinting mechanism in large ensemble
434 simulations of the second generation Canadian earth system model: uncertainty due
435 to internal climate variability. *Climate Dynamics*, *55*(9–10), 2523–2541.
436 <https://doi.org/10.1007/s00382-020-05396-y>

437 Clement, A., DiNezio, P., & Deser, C. (2011). Rethinking the ocean’s role in the Southern
438 Oscillation. *Journal of Climate*, *24*(15), 4056–4072.
439 <https://doi.org/10.1175/2011JCLI3973.1>

440 Czaja, A., van der Vaart, P., & Marshall, J. (2002). A diagnostic study of the role of remote
441 forcing in tropical Atlantic variability. *Journal of Climate*, *15*(22), 3280–3290.
442 [https://doi.org/10.1175/1520-0442\(2002\)015<3280:ADSOTR>2.0.CO;2](https://doi.org/10.1175/1520-0442(2002)015<3280:ADSOTR>2.0.CO;2)

443 Deser, C., Sun, L., Tomas, R. A., & Screen, J. (2016). Does ocean coupling matter for the
444 northern extratropical response to projected Arctic sea ice loss? *Geophysical
445 Research Letters*, *43*(5), 2149–2157. <https://doi.org/10.1002/2016GL067792>

446 Dittus, A. J., Hawkins, E., Robson, J. I., Smith, D. M., & Wilcox, L. J. (2021). Drivers of
447 Recent North Pacific Decadal Variability: The Role of Aerosol Forcing. *Earth’s Future*,
448 *9*(12). <https://doi.org/10.1029/2021EF002249>

449 Dow, W. J., Maycock, A. C., Lofverstrom, M., & Smith, C. J. (2021). The effect of
450 anthropogenic aerosols on the aleutian low. *Journal of Climate*, *34*(5), 1725–1741.
451 <https://doi.org/10.1175/JCLI-D-20-0423.1>

452 Gan, B. L. Wu, F Jia, S. Li, W. Cai, H. Nakamura, M. A. Alexander, and A. J. Miller,
453 2017: On the response of the Aleutian Low to greenhouse warming. *J. Climate*,
454 *30*, 3907–3925, doi: 10.1175/JCLI-D-15-0789.1

455 Gu, D., & Philander, S. G. H. (1997). Interdecadal climate fluctuations that depend on
456 exchanges between the tropics and extratropics. *Science*, 275(5301), 805–807.
457 <https://doi.org/10.1126/science.275.5301.805>

458 Hu, D., & Guan, Z. (2018). Decadal relationship between the stratospheric arctic vortex and
459 pacific decadal oscillation. *Journal of Climate*, 31(9), 3371–3386.
460 <https://doi.org/10.1175/JCLI-D-17-0266.1>

461 Jin, F. F. (2001). Low-frequency modes of tropical ocean dynamics. *Journal of Climate*,
462 14(18), 3874–3881. [https://doi.org/10.1175/1520-
463 0442\(2001\)014<3874:LFMOTO>2.0.CO;2](https://doi.org/10.1175/1520-0442(2001)014<3874:LFMOTO>2.0.CO;2)

464 Joshi, M., Hall, R. A., Stevens, D. P., and Hawkins, E.: The modelled climatic response
465 to the 18.6-year lunar nodal cycle and its role in decadal temperature trends, *Earth*
466 *Syst. Dynam.*, 14, 443–455, <https://doi.org/10.5194/esd-14-443-2023>, 2023.

467 Joshi, M., Stringer, M., Van Der Wiel, K., O’Callaghan, A., & Fueglistaler, S. (2015).
468 IGCM4: A fast, parallel and flexible intermediate climate model. *Geoscientific Model*
469 *Development*, 8(4), 1157–1167. <https://doi.org/10.5194/gmd-8-1157-2015>

470 Klavans et al. (2023) Recent Atlantic multidecadal variability and its impacts are driven by
471 external forcings, submitted

472 Knight, J. R., Maidens, A., Watson, P. A. G., Andrews, M., Belcher, S., Brunet, G.,
473 Fereday, D., Folland, C. K., Scaife, A. A., & Slingo, J. (2017). Global meteorological
474 influences on the record UK rainfall of winter 2013-14. *Environmental Research*
475 *Letters*, 12(7). <https://doi.org/10.1088/1748-9326/aa693c>

476 Knutson, T. R., & Manabe, S. (1998). Model assessment of decadal variability and trends
477 in the tropical Pacific Ocean. In *Journal of Climate* (Vol. 11, Issue 9).
478 [https://doi.org/10.1175/1520-0442\(1998\)011<2273:MAODVA>2.0.CO;2](https://doi.org/10.1175/1520-0442(1998)011<2273:MAODVA>2.0.CO;2)

479 Kwon, Y. O., & Deser, C. (2007). North Pacific decadal variability in the community climate
480 system model version 2. *Journal of Climate*, 20(11), 2416–2433.
481 <https://doi.org/10.1175/JCLI4103.1>

- 482 Latif, M., & Barnett, T. P. (1996). Decadal climate variability over the North Pacific and
483 North America: Dynamics and predictability. *Journal of Climate*, 9(10), 2407–2423.
484 [https://doi.org/10.1175/1520-0442\(1996\)009<2407:DCVOTN>2.0.CO;2](https://doi.org/10.1175/1520-0442(1996)009<2407:DCVOTN>2.0.CO;2)
- 485 Liguori, G., & Di Lorenzo, E. (2019). Separating the North and South Pacific Meridional
486 Modes Contributions to ENSO and Tropical Decadal Variability. *Geophysical*
487 *Research Letters*, 46(2), 906–915. <https://doi.org/10.1029/2018GL080320>
- 488 Litzow, M. A., Malick, M. J., Bond, N. A., Cunningham, C. J., Gosselin, J. L., & Ward, E. J.
489 (2020). Quantifying a Novel Climate Through Changes in PDO-Climate and PDO-
490 Salmon Relationships. *Geophysical Research Letters*, 47(16), e2020GL087972.
491 <https://doi.org/10.1029/2020GL087972>
- 492 Liu, Y., Sun, C., Kucharski, F., Li, J., Wang, C., & Ding, R. (2021). The North Pacific Blob
493 acts to increase the predictability of the Atlantic warm pool. *Environmental Research*
494 *Letters*, 16(6), 064034. <https://doi.org/10.1088/1748-9326/ac0030>
- 495 Lysne, J. A., Chang, P., & Giese, B. (1997). Impact of the extratropical Pacific on equatorial
496 variability. *Geophysical Research Letters*, 24(21), 2589–2592.
497 <https://doi.org/10.1029/97GL02751>
- 498 Mantua, N. J., Hare, S. R., Zhang, Y., Wallace, J. M., & Francis, R. C. (1997). A Pacific
499 Interdecadal Climate Oscillation with Impacts on Salmon Production. *Bulletin of the*
500 *American Meteorological Society*, 78(6), 1069–1079. [https://doi.org/10.1175/1520-
501 0477\(1997\)078<1069:APICOW>2.0.CO;2](https://doi.org/10.1175/1520-0477(1997)078<1069:APICOW>2.0.CO;2)
- 502 Mahajan, S., Saravanan, R., & Chang, P. (2009). The role of the wind-evaporation-sea
503 surface temperature (WES) feedback in air-sea coupled tropical variability.
504 *Atmospheric Research*, 94(1), 19–36. <https://doi.org/10.1016/j.atmosres.2008.09.017>
- 505 Martin, Z., Orbe, C., Wang, S., & Sobel, A. (2021). The MJO–QBO relationship in a GCM
506 with stratospheric nudging. *Journal of Climate*, 34(11), 4603–4624.
507 <https://doi.org/10.1175/JCLI-D-20-0636.1>
- 508 McCreary, J. P., & Peng Lu. (1994). Interaction between the subtropical and equatorial
509 ocean circulations: the subtropical cell. *Journal of Physical Oceanography*, 24(2),
510 466–497. [https://doi.org/10.1175/1520-0485\(1994\)024<0466:IBTSAE>2.0.CO;2](https://doi.org/10.1175/1520-0485(1994)024<0466:IBTSAE>2.0.CO;2)

- 511 Nagano, A., & Wakita, M. (2019). Wind-driven decadal sea surface height and main
512 pycnocline depth changes in the western subarctic North Pacific. *Progress in Earth
513 and Planetary Science*, 6(1), 1–26. <https://doi.org/10.1186/s40645-019-0303-0>
- 514 Newman, M., Alexander, M. A., Ault, T. R., Cobb, K. M., Deser, C., Di Lorenzo, E., Mantua,
515 N. J., Miller, A. J., Minobe, S., Nakamura, H., Schneider, N., Vimont, D. J., Phillips, A.
516 S., Scott, J. D., & Smith, C. A. (2016). The Pacific decadal oscillation, revisited.
517 *Journal of Climate*, 29(12), 4399–4427. <https://doi.org/10.1175/JCLI-D-15-0508.1>
- 518 Pickart, R. S., Moore, G. W. K., Macdonald, A. M., Renfrew, I. A., Walsh, J. E., & Kessler,
519 W. S. (2009). Seasonal evolution of Aleutian low pressure systems: Implications for
520 the North Pacific subpolar circulation. *Journal of Physical Oceanography*, 39(6),
521 1317–1339. <https://doi.org/10.1175/2008JPO3891.1>
- 522 Pierce, D. W., Barnett, T. P., & Latif, M. (2000). Connections between the Pacific Ocean
523 Tropics and midlatitudes on decadal timescales. *Journal of Climate*, 13(6), 1173–
524 1194. [https://doi.org/10.1175/1520-0442\(2000\)013<1173:CBTPOT>2.0.CO;2](https://doi.org/10.1175/1520-0442(2000)013<1173:CBTPOT>2.0.CO;2)
- 525 Richter, J. H., Deser, C., & Sun, L. (2015). Effects of stratospheric variability on El Niño.
526 *Environmental Research Letters*, 10(12). [https://doi.org/10.1088/1748-
527 9326/10/12/124021](https://doi.org/10.1088/1748-9326/10/12/124021)
- 528 Schneider, N., & Cornuelle, B. D. (2005). The forcing of the Pacific Decadal Oscillation.
529 *Journal of Climate*, 18(21), 4355–4373. <https://doi.org/10.1175/JCLI3527.1>
- 530 Schneider, N., Miller, A. J., & Pierce, D. W. (2002). Anatomy of North Pacific decadal
531 variability. In *Journal of Climate* (Vol. 15, Issue 6). [https://doi.org/10.1175/1520-
532 0442\(2002\)015<0586:AONPDV>2.0.CO;2](https://doi.org/10.1175/1520-0442(2002)015<0586:AONPDV>2.0.CO;2)
- 533 Simon, A., Gastineau, G., Frankignoul, C., Rousset, C., & Codron, F. (2021). Transient
534 climate response to Arctic Sea ice loss with two ice-constraining methods. *Journal of
535 Climate*, 34(9), 3295–3310. <https://doi.org/10.1175/JCLI-D-20-0288.1>
- 536 Smith, D. M., Booth, B. B. B., Dunstone, N. J., Eade, R., Hermanson, L., Jones, G. S.,
537 Scaife, A. A., Sheen, K. L., & Thompson, V. (2016). Role of volcanic and
538 anthropogenic aerosols in the recent global surface warming slowdown. *Nature
539 Climate Change*, 6(10), 936–940. <https://doi.org/10.1038/nclimate3058>

540 Sugimoto, S., & Hanawa, K. (2009). Decadal and interdecadal variations of the Aleutian
541 Low activity and their relation to upper oceanic variations over the North Pacific.
542 *Journal of the Meteorological Society of Japan*, 87(4), 601–614.
543 <https://doi.org/10.2151/jmsj.87.601>

544 Sun, J., & Wang, H. (2006). Relationship between Arctic Oscillation and Pacific Decadal
545 Oscillation on decadal timescale. *Chinese Science Bulletin*, 51(1), 75–79.
546 <https://doi.org/10.1007/s11434-004-0221-3>

547 Sun, T., & Okumura, Y. M. (2019). Role of stochastic atmospheric forcing from the south
548 and North Pacific in tropical Pacific decadal variability. *Journal of Climate*, 32(13),
549 4013–4038. <https://doi.org/10.1175/JCLI-D-18-0536.1>

550 Taguchi, B., Xie, S. P., Schneider, N., Nonaka, M., Sasaki, H., & Sasai, Y. (2007). Decadal
551 variability of the Kuroshio Extension: Observations and an eddy-resolving model
552 hindcast. *Journal of Climate*, 20(11), 2357–2377. <https://doi.org/10.1175/JCLI4142.1>

553 Trenberth, K. E., & Hurrell, J. W. (1994). Decadal atmosphere-ocean variations in the
554 Pacific. *Climate Dynamics*, 9(6), 303–319. <https://doi.org/10.1007/BF00204745>

555 Vimont, D. J. (2005). The contribution of the interannual ENSO cycle to the spatial pattern
556 of decadal ENSO-like variability. In *Journal of Climate* (Vol. 18, Issue 12).
557 <https://doi.org/10.1175/JCLI3365.1>

558 Vimont, D. J., Battisti, D. S., & Hirst, A. C. (2001). Footprinting: A seasonal connection
559 between the tropics and mid-latitudes. *Geophysical Research Letters*, 28(20), 3923–
560 3926. <https://doi.org/10.1029/2001GL013435>

561 Vimont, D. J., Battisti, D. S., & Hirst, A. C. (2002). Pacific interannual and interdecadal
562 equatorial variability in a 1000-Yr simulation of the CSIRO coupled general circulation
563 model. *Journal of Climate*, 15(2), 160–178. [https://doi.org/10.1175/1520-
564 0442\(2002\)015<0160:PIAIEV>2.0.CO;2](https://doi.org/10.1175/1520-0442(2002)015<0160:PIAIEV>2.0.CO;2)

565 Vimont, D. J., Wallace, J. M., & Battisti, D. S. (2003). The seasonal footprinting mechanism
566 in the Pacific: Implications for ENSO. *Journal of Climate*, 16(16), 2668–2675.
567 [https://doi.org/10.1175/1520-0442\(2003\)016<2668:TSMIT>2.0.CO;2](https://doi.org/10.1175/1520-0442(2003)016<2668:TSMIT>2.0.CO;2)

568 Wang, H., Kumar, A., Wang, W., & Xue, Y. (2012). Seasonality of the Pacific decadal
569 oscillation. *Journal of Climate*, 25(1), 25–38. <https://doi.org/10.1175/2011JCLI4092.1>

570 Watson, P. A. G., Weisheimer, A., Knight, J. R., & Palmer, T. N. (2016). The role of the
571 tropical West Pacific in the extreme Northern Hemisphere winter of 2013/2014.
572 *Journal of Geophysical Research*, 121(4), 1698–1714.
573 <https://doi.org/10.1002/2015JD024048>

574 Webb, D. J. (1996). An ocean model code for array processor computers. *Computers and*
575 *Geosciences*, 22(5), 569–578. [https://doi.org/10.1016/0098-3004\(95\)00133-6](https://doi.org/10.1016/0098-3004(95)00133-6)

576 Wills, R. C. J., Battisti, D. S., Proistosescu, C., Thompson, L. A., Hartmann, D. L., &
577 Armour, K. C. (2019). Ocean Circulation Signatures of North Pacific Decadal
578 Variability. *Geophysical Research Letters*, 46(3), 1690–1701.
579 <https://doi.org/10.1029/2018GL080716>

580 Xie, S. P., & Tanimoto, Y. (1998). A pan-Atlantic decadal climate oscillation. *Geophysical*
581 *Research Letters*, 25(12), 2185–2188. <https://doi.org/10.1029/98GL01525>

582 Zhang, D., & McPhaden, M. J. (2006). Decadal variability of the shallow Pacific meridional
583 overturning circulation: Relation to tropical sea surface temperatures in observations
584 and climate change models. *Ocean Modelling*, 15(3–4), 250–273.
585 <https://doi.org/10.1016/j.ocemod.2005.12.005>

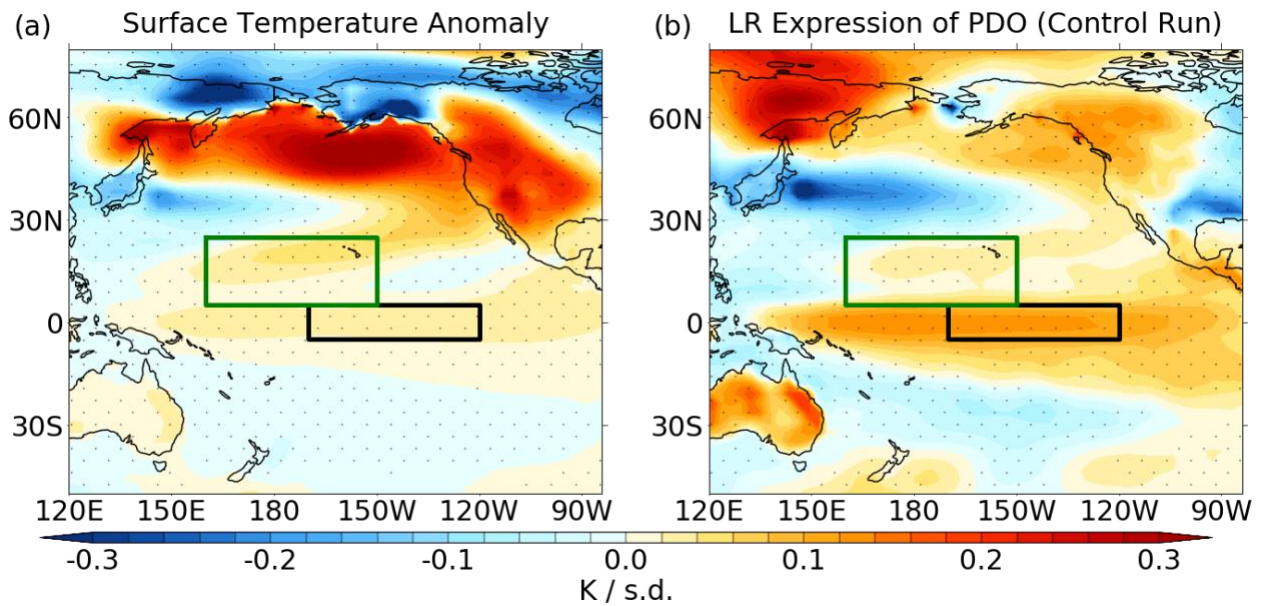
586 Zhang, Y., Xie, S. P., Kosaka, Y., & Yang, J. C. (2018). Pacific decadal oscillation: Tropical
587 Pacific forcing versus internal variability. *Journal of Climate*, 31(20), 8265–8279.
588 <https://doi.org/10.1175/JCLI-D-18-0164.1>

589 Zhao, Y., Newman, M., Capotondi, A., Lorenzo, E. Di, & Sun, D. (2021). Removing the
590 effects of tropical dynamics from north pacific climate variability. *Journal of Climate*,
591 34(23), 9249–9265. <https://doi.org/10.1175/JCLI-D-21-0344.1>

592
593
594
595
596

597 **Figures**

598

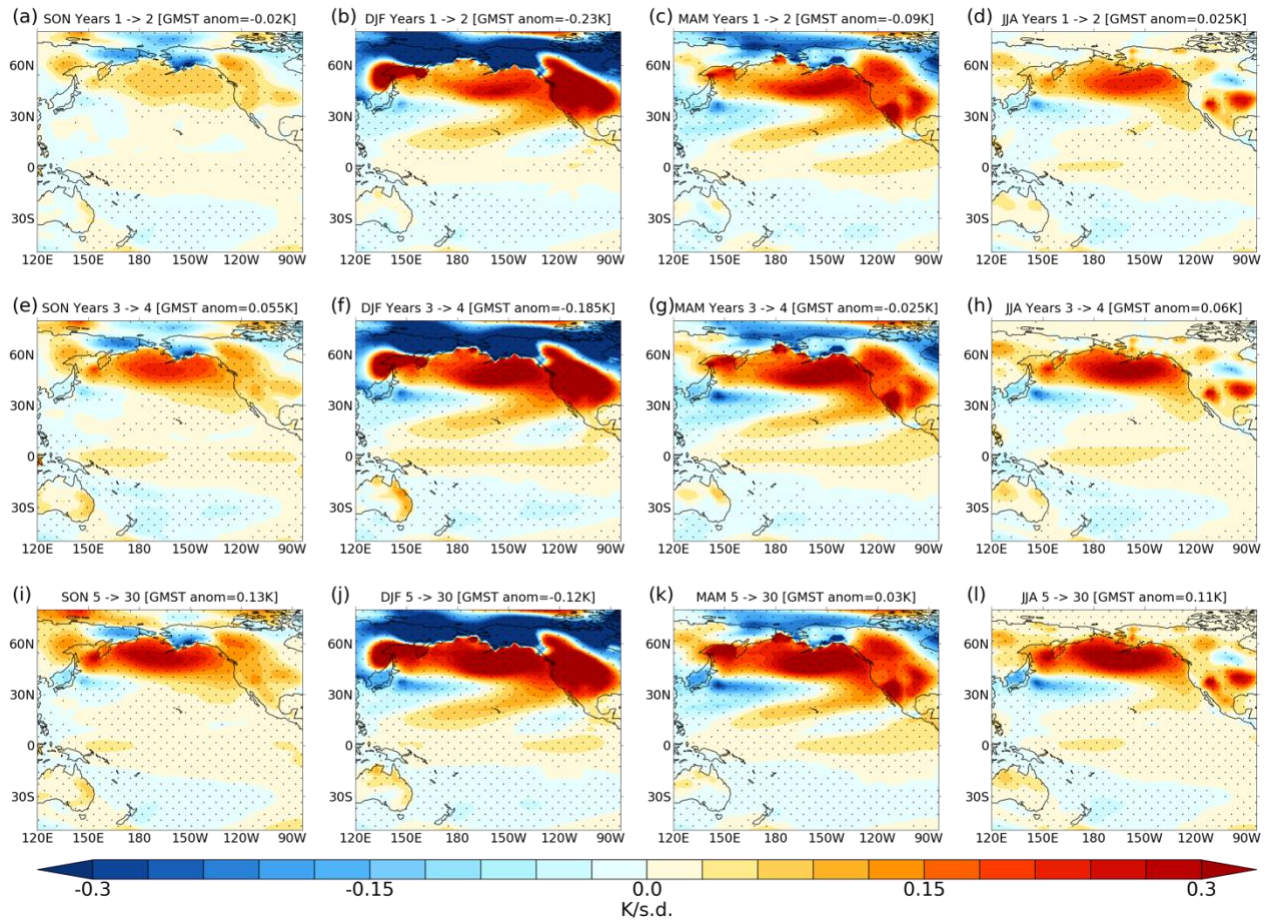


599

600 **Figure 1:** Annual mean surface temperature anomalies for (a) ensemble mean anomaly
601 in NUDGED averaged over years 1-30; (b) linear regression (LR) onto the PDO index in
602 CONTROL. The anomaly between NUDGED and CONTROL is projected onto the first
603 EOF from the control run to generate a pseudo-PC. The anomaly is divided by the
604 pseudo-PC to calculate the anomaly per standard deviation of the PDO index, expressed
605 in a similar way to that derived from CONTROL. Units are K per standard deviation.
606 Stippling denotes anomalies that are significant at the 95% level. Green and black boxes
607 show the regions for the mixed layer heat budget analysis.

608

609



610

611

612 **Figure 2:** Seasonal mean surface temperature anomalies in NUDGED expressed per
 613 unit PDO index [K/σ] for SON, DJF, MAM and JJA. Composite anomalies are shown for
 614 years 1-2 (a-d), years 3-4 (e-h) and years 5-30 (i-l). Global mean surface temperature
 615 anomalies are shown in the header. Stippling denotes anomalies that are significant at
 616 the 95% level.

617

618

619

620

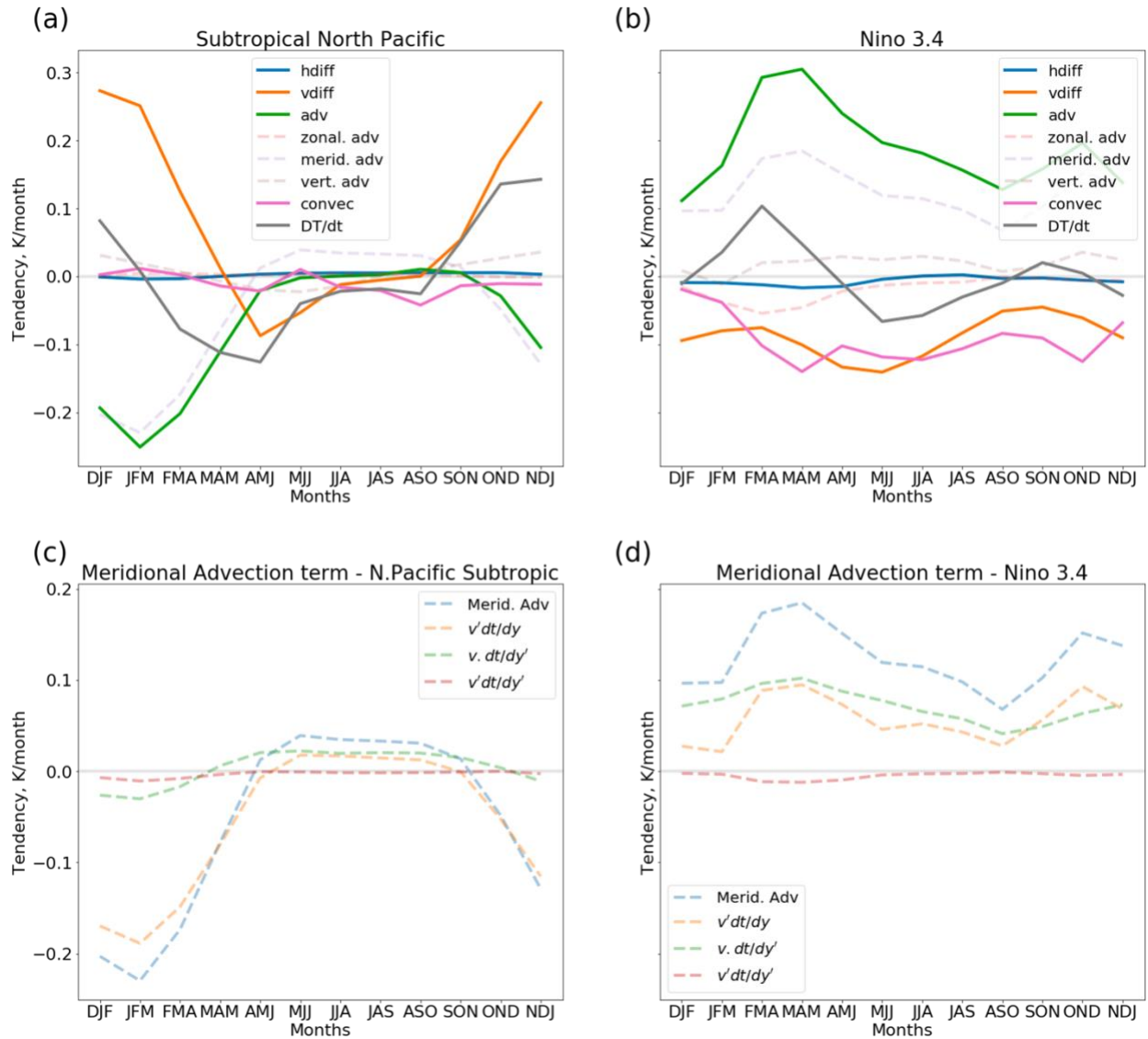
621

622

623

624

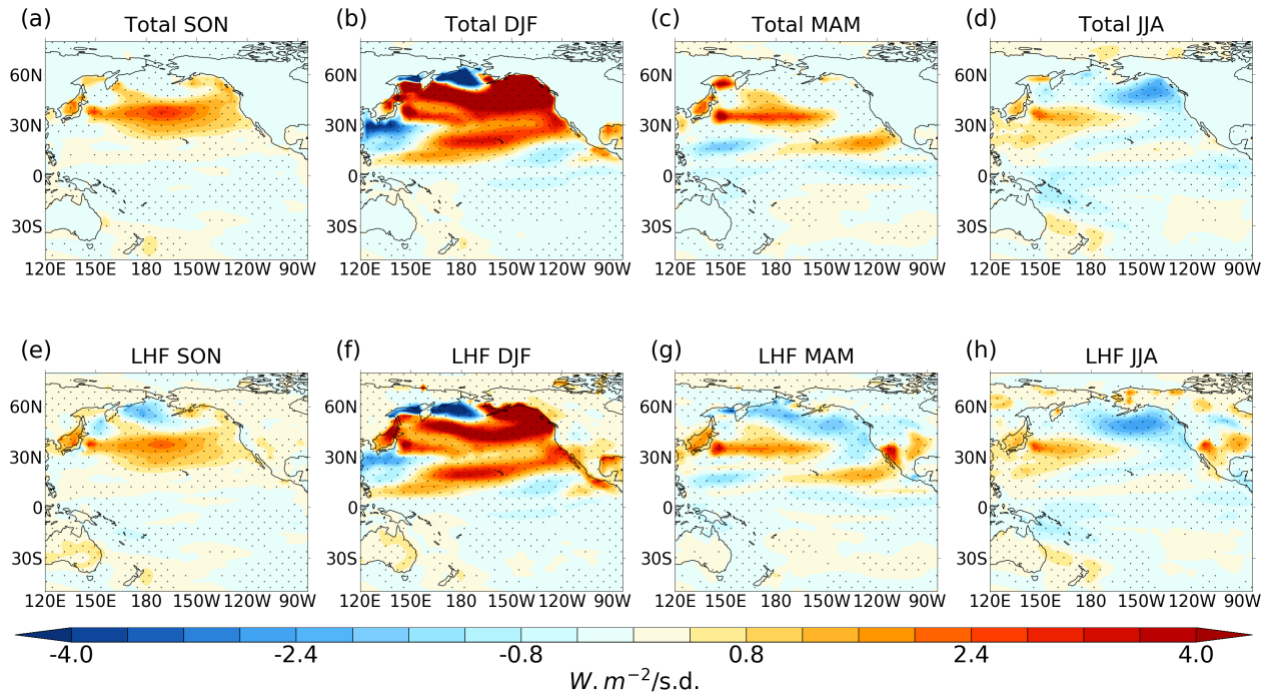
625



626
627

628 **Figure 3:** Years 1-30, 3-month moving average of anomalous NUDGED minus
629 CONTROL mixed layer temperature tendencies and constituent heat budget terms for the
630 (a) subtropical North Pacific and (b) Niño 3.4 regions. (c,d) show the meridional advection
631 term and its linear expansion. The subtropical North Pacific and Niño 3.4 domains are
632 indicated by the boxes in Fig. 1.

633
634



635

636

637 **Figure 4:** (a-d) Years 1-30 seasonal mean net surface heat flux anomalies in NUDGED.

638 (e-h): Years 1-30 seasonal mean latent heat flux anomaly in NUDGED. Positive denotes

639 downward flux. Stippling denotes anomalies that are statistically significant at the 95%

640 level. Units: $W \cdot m^{-2}$ per standard deviation.

641

642

643

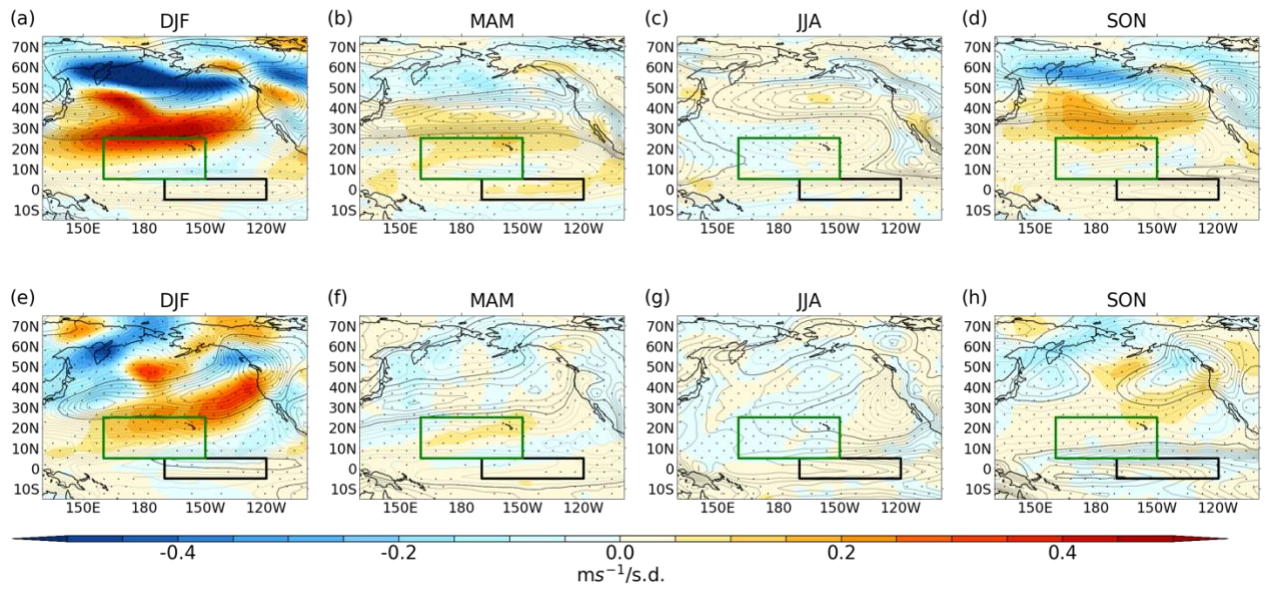
644

645

646

647

648



649

650 **Figure 5:** Years 1-30 seasonal mean NUDGED-CONTROL near-surface (lowest model
 651 level) wind anomalies for (a-d) zonal and (e-h) meridional wind. Contours show
 652 climatology of CONTROL (dashed lines are negative values, contour interval 1 m s^{-1}).
 653 Stippling denotes anomalies that are significant at the 95% level.

654

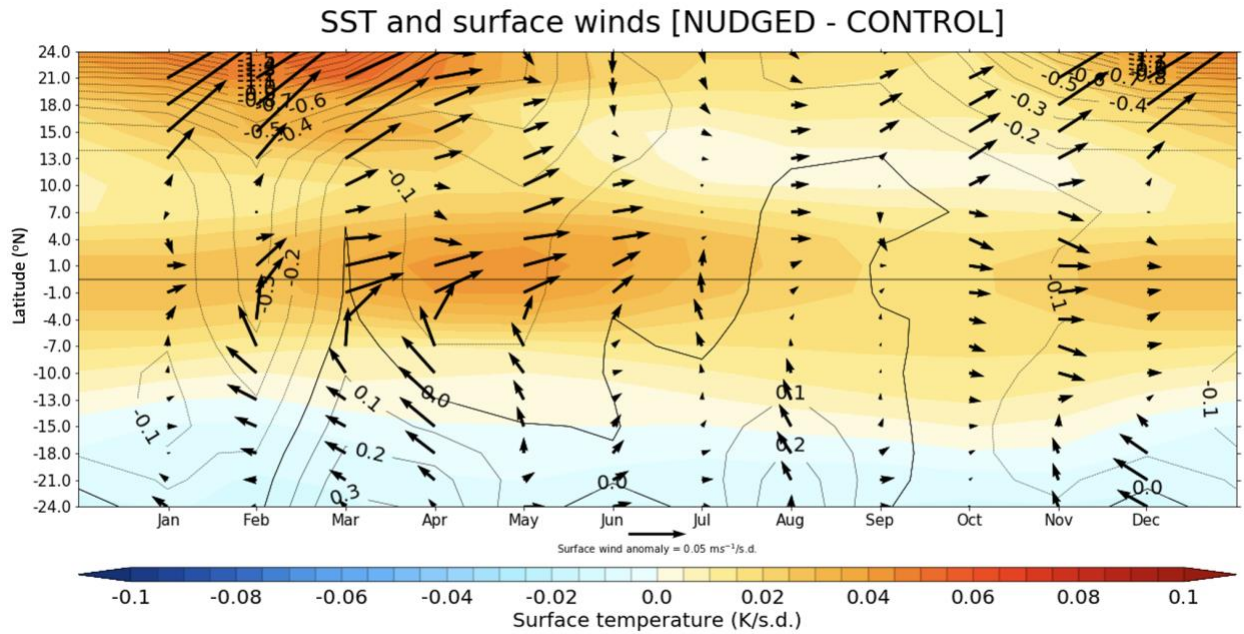
655

656

657

658

659



660

661

662 **Figure 6:** Years 1-30 latitude-time section of NUDGED minus CONTROL SST anomaly
 663 (K/ σ : shading), surface pressure (hPa/ σ : contours) and near-surface wind anomaly (m s⁻¹/
 664 σ : vectors) averaged over the central-eastern tropical Pacific (205°W-80°W).

665

666

667

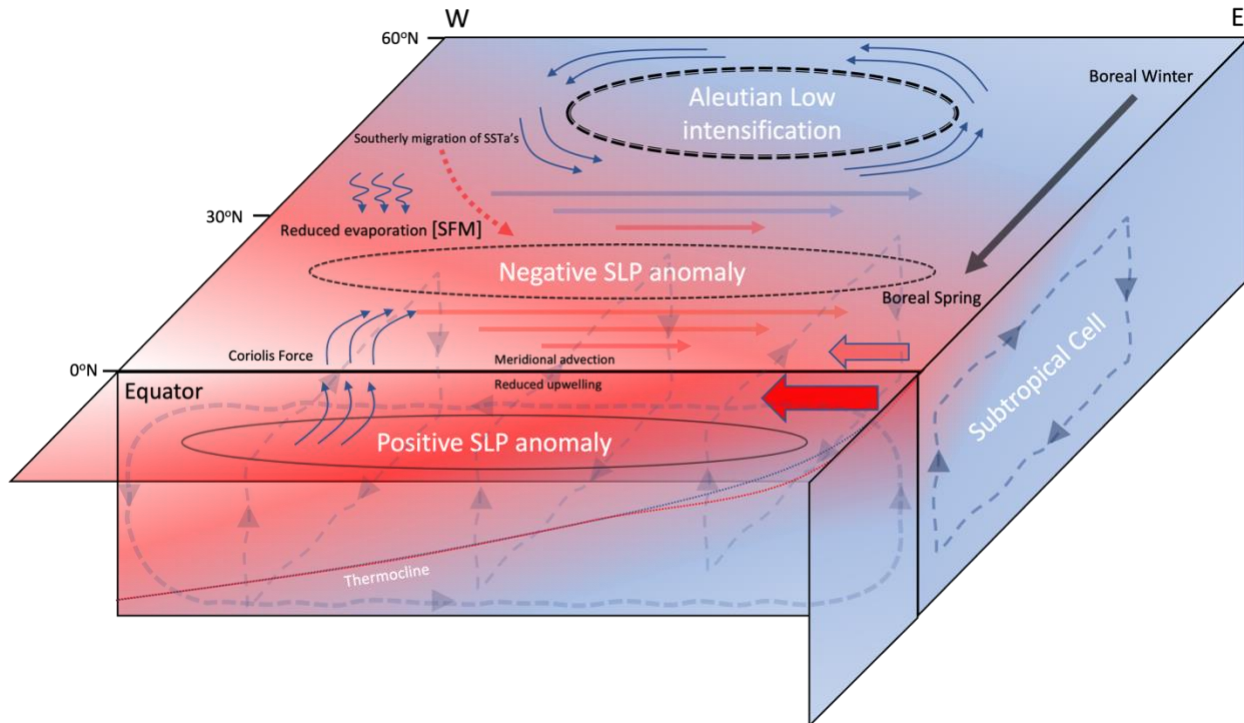
668

669

670

671

672



673
 674 **Figure 7:** Schematic depicting the mechanisms involved in the tropical SST anomalies
 675 manifest as a result from an intensification of the AL. An intensified AL (dashed black
 676 line) imposed during boreal winter is associated with intensified westerlies (reduced
 677 easterlies; solid arrows) in the subtropics and downward latent heat transfer. The
 678 migration of the SST anomalies southward during boreal winter is associated with
 679 westerly anomalies in the subtropics (reduced trades). The westerly anomalies act to
 680 weaken the background trades (filled red arrow) which reduces latent heating cooling
 681 due to decreased evaporation and hence an increase in subtropical Pacific SSTs. In the
 682 season after nudging, the temperature asymmetry about the equator induces an SLP
 683 gradient (solid line – positive SLP; dashed line – negative SLP) that drives southerly
 684 winds across the equator. The Coriolis force acts to turn the southerly winds in the
 685 southern hemisphere westward and in the northern hemisphere eastward. When these
 686 anomalous winds are imposed on the background easterly trade winds (filled red
 687 arrows), the southerlies south of the equator increase the wind speed and therefore
 688 evaporative cooling, whilst north of the equator the background trades are weakened,
 689 reducing evaporative cooling. The westerly wind anomalies along the equator deepen

690 the thermocline in the eastern tropical Pacific (red dotted line) and reduce
691 upwelling/divergence of cooler waters at the equator.

692

693

694

695